Experimental study of a quadrirotor twin vertical axis tidal turbine behaviour under regular waves

Y. Saouli, B. Gaurier, G. Germain, R. Linant and G. Maurice

***Abstract*—The consideration of the environmental conditions on the power output of vertical-axis tidal turbines (VATT) is a key aspect in assessing their in-situ performance and ensuring stable energy production, as well as a satisfactory lifespan. This study presents an experimental analysis of the surface waves effect on the mechanical response (power and torque fluctuations) of a quadrirotor VATT. Tests were conducted in Ifremer's wave-current flume tank on a 1:20 scale model. The results highlight a significant increase in power fluctuations under regular waves, particularly near the optimal operating point. Moreover, the phase-averaged modelling of the wave-induced torque variations reveals a strong relationship between wave-induced velocity fluctuations and torque response. A parametric model, inspired by Morison's equation to represent the inertial effects of waves on the machine, effectively captures the wave-related torque contribution. The proposed method thus aims to distinguish wave orbital velocity effects to the turbulence-induced fluctuations.**

***Index Terms*—Vertical axis, Tidal turbine, Experimental, Waves.**

I. Introduction

THE large-scale deployment of tidal turbines for energy production depends on a thorough understanding of their behaviour under real operating conditions. Among the whole concepts of machines, vertical-axis tidal turbines (VATT) provide various advantages in complex flow environments, particularly in shallow-water sites [1]. In such environments, the interaction between waves and current is a major factor influencing turbine performance [2]. This phenomenon is particularly relevant in high-energy tidal sites open to the sea, where surface waves induce unsteady flow conditions. Understanding these interactions is therefore crucial for optimizing energy production and ensuring the long-term reliability of tidal turbines.

Previous studies on horizontal axis turbines [3], [4], [5] show that the waves generate periodic fluctuations in flow velocity and structure loading, affecting both power output and mechanical stress. Similar effects have been observed in vertical-axis turbines as reported in experimental studies [6]. These fluctuations can lead to fatigue damage, unsteady hydrodynamic forces, and wake instabilities which ultimately influence the performance and the lifetime of tidal turbines. Developing a comprehensive understanding of these effects is essential for improving turbine design and optimizing control strategies [7] under realistic sea conditions.

To develop knowledge about vertical axis turbines, the joint laboratory Verti-Lab was created between Ifremer and Hydroquest, combining experimental, numerical and in-situ investigations. It builds upon previous experimental work [8]- [9], demonstrating the ability to accurately replicate the turbines response at a reduced scale. Among the various studies carried out in this context, this study presents an experimental approach to quantify the impact of wave-induced velocity fluctuations on the power production of a new generation of turbines designed by HydroQuest (1:20 scale model in Fig. 1).

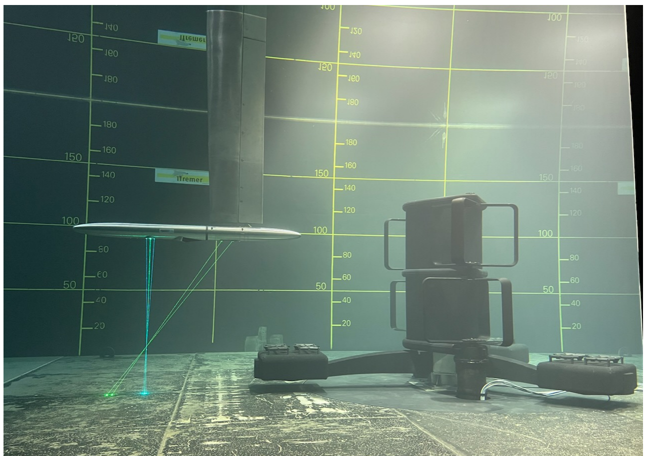

Fig. 1. Reduced-scale turbine model in the Ifremer flume tank, with the 3C-LDV probe placed upstream from the turbine for induction measurements.

In this paper, the experimental setup used for the tests is first presented. Then, the turbine response in

Part of a special issue for EWTEC 2025. Original version published in EWTEC 2025 proceedings at doi.org/10.36688/ewtec-2025-804.

This paper has been subject to single-blind peer review by a minimum of two reviewers.

This work received the financial support of the French Agence Nationale de la Recherche through the Verti-Lab project (ANR-23-LCV1-0009-01), the French Research and Technology National Association (ANRT) under the convention Cifre n° 2023/0217 and the CPER IDEAL.

Y. Saouli and R. Linant are with HydroQuest SAS and the French Research Institute for the Exploitation of the Sea (IFREMER) Centre Manche Mer du Nord, Boulogne-sur-Mer FR-62321, France. (e-mail: yanis.saouli@ifremer.fr)

G. Germain, B. Gaurier are with the French Research Institute for the Exploitation of the Sea (IFREMER) Centre Manche Mer du Nord, Boulogne-sur-Mer FR-62321, France. (e-mail: gregory.germain@ifremer.fr).

G. Maurice is with HydroQuest SAS, 16 Chemin de Malacher, Meylan FR-38240, France. (e-mail: guillaume.maurice@hydroquest.net).

Digital Object Identifier: https://doi.org/10.36688/imej.9.55-64

terms of performance and torque distribution under wave forcing is investigated. The wave contribution is highlighted and reconstructed using the RAO approach. Finally, a parametric formulation inspired by Morison's equation is tested to represent torque fluctuations.

II. Experimental facility

A. Description of the model

The studied model is the 1:20th prototype of the 2.5 MW-rated machines planned to be deployed in the context of the FloWatt project (in the Raz-Blanchard, France). This model, named OQ 2.5, consists of two vertical axis rotor columns, also made of two levels of rotors that are 60° out of phase. Its dimensions are defined in order to follow the geometric similarity in the tank, and therefore to respect the ratio between the height of the machine and the tank depth.

The model is H_m= 1.010 m high, for a width including rotors of w_m = 1.270 m. Each rotor is H_b = 0.315 m and R = 0.235 m, respectively for the height and the radius. The distance between the bottom plate and the top plate holding the rotor columns determines the turbine height: h_m = 0.830 m. The gravity base is composed of three lested arms, fixed to the anchor base. The arm going upstream is placed along the flow axis for this study (see Fig. 2).

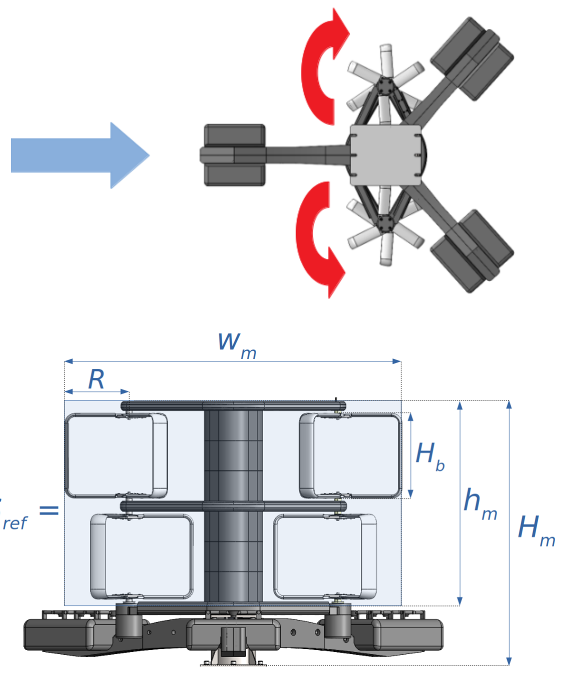

Fig. 2. Model's characteristics. Top: rotation directon of each rotor column and flow direction (blue arrow). Bottom: main dimensions of the model.

The driving system is installed in blocks located under the two columns, they include a 26:1 geared motor and a torquemeter set to a sampling frequency $f_e = 512$ Hz. The system is controlled at a set rotational speed ω (for an equivalent rotational frequency f_ω). Fig. 2 defines the reference surface taken as the indicated blue zone, representing the turbine projected capture area $S_{ref} = h_m \times w_m$. An equivalent diameter D_e is derived from this surface, established from the International Electrotechnical Commission norms : $D_e = \sqrt{\frac{4S_{ref}}{\pi}}$, which is used to transform a non-circular cross-section machine into an equivalent device with a circular cross-section.

B. Flume tank setup

The OQ 2.5 model is tested in the wave and current circulating tank of Ifremer situated in Boulogne-sur-Mer (France). The test section is 18 m long × 4 m wide × 2 m deep (h = 2 m, see Fig. 3). The three instantaneous velocity components are denoted (U, V, W) along the (x, y, z) directions respectively, with x the main flow direction as displayed in the schematic. The flow velocity reference is evaluated from measurements carried out far upstream of the turbine to avoid the inductive effects of the turbine. It is noted (U_0, V_0, W_0), with flow velocity values of U_0 = 0.89 m/s and $V_0 = W_0 = 0$ m/s. The model is installed at the centre of the tank, the x-origin is set as displayed in Fig. 3 and with z = 0 to the tank floor. The turbine is centred in the span-wise direction of the tank, with the span-wise origin (y = 0) set to the centre of the model, and so of the tank. The operating point of the turbine is defined from its Tip Speed Ratio $TSR = \frac{\omega.R}{U_0}$. Thanks to a grid combined with a honeycomb placed at the inlet of the working section, a low turbulence intensity TI_0 = 1.5 % is reached with current only [10]. The boundary layer height is calculated as follows: $\delta_{95} = 0.95 \times U_0 \approx 0.250$ m. The expression of the flow velocity components follows the Reynolds decomposition :

$$U(t) = \overline{U} + u_{wave}(t) + u'(t) \quad (1)$$

with $\overline{U}$ the mean component, $u_{wave}(t)$ the orbital velocity fluctuations and $u'(t)$ the turbulent part of the flow velocity. The wave-related velocity is defined as $U_{wave}(t) = \overline{U} + u_{wave}(t)$.

To study the wave-current interaction, a wave-maker and a wave-absorber are used in order to generate waves following the current, with the wave-maker placed at the inlet of the working section. The wave-absorber is made of a metallic porous panel (8% porosity) and is set to reduce wave reflection on the outlet wall of the working section.

A combination of six wave gauges, three resistive wave probes and three KENEK servo-type wave probes (dynamic probes), is used to measure the surface elevation in the flume tank. One of the dynamic wave probes is set on the top of the machine (x = 0, gauge C on the scheme) and composes the reference surface elevation measurements related to the following results. The measurements are synchronised with the torquemeter, i.e. are carried out at a sampling frequency of f_e = 512 Hz. In addition, to evaluate the experimental orbital velocity, PIV measurements are carried out upstream of the rotor column. The measurements are made using cameras HisenseZyla 5.5M pixels, with a greyscale coding parameter of 16 bits for each pixel. The sampling frequency is set at f_s = 15 Hz. The size of the vertical PIV planes cover the

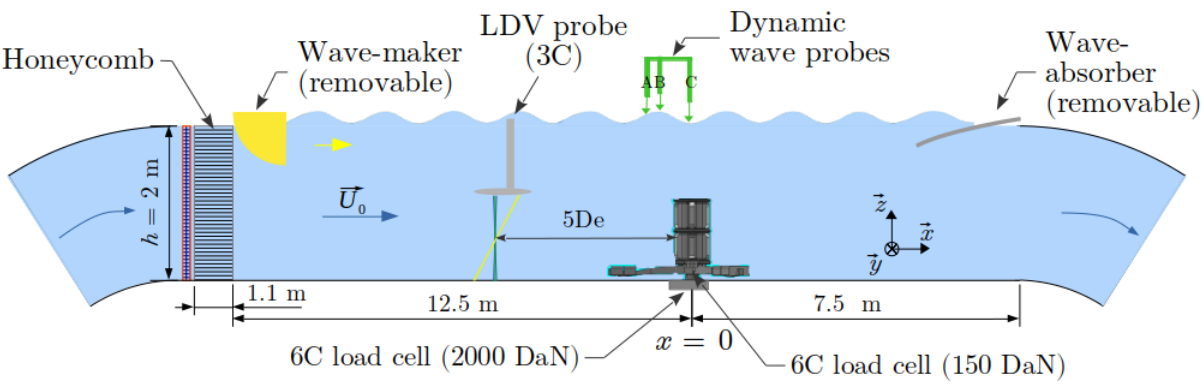

Fig. 3. Schematic description of the flume tank, the turbine location and the instrumentation used (wave probes, load cells and laser techniques) during the tests. The wavemaker is installed at the inlet of the working section, generating waves following the current.

column height and the x-positions from x/D_e = -0.70 to x/D_e = -0.15. The spatial resolution is $dx = dz$ = 13 mm.

C. Studied wave cases

Three experimental wave cases are presented in this part. The waves propagate in the same direction as the current. Each test lasts 120 seconds, corresponding to 54 wave cycles for cases with f_{wave} = 0.60 Hz and 40 wave cycles for cases with f_{wave} = 0.45 Hz (f_{wave} is defined as the wave frequency), as we work on the time range for which the waves are fully established (from t = 30 s to t = 120 s). The wavelength and the wave amplitude are thus determined from the wave gauges measurements and are given in Table I. The in-situ equivalent wave conditions, representative of typical wave events in the Raz-Blanchard (Alderney Race) [11], are presented in Table I in brackets.

Based on the geometric similarity and to ensure wave dynamic similarity between the full-scale and tank conditions, the Froude number is preserved, validating the correct reproduction of wave effects in the experimental setup. Additional dimensionless parameters, such as the Keulegan-Carpenter number and the relative wave height-to-water depth ratio, are also considered. In all cases, the wave height-to-depth ratio remains below 0.1, justifying the use of Airy wave theory for modeling wave kinematics in the following.

$$KC = \frac{U_{wave}\,T}{D_e} \qquad F_r = \frac{U_0}{\sqrt{g(h - H_m)}} \tag{2}$$

In Fig. 4 (top), the probability density function (PDF) of wave amplitudes is fit with a Gaussian model, from which the average wave crest amplitude (a) and its standard deviation $\sigma(a)$ are extracted. These values are taken from the wave probe measurements positioned vertically above the turbine. The standard deviation remains around 15% for all wave cases, indicating steady wave conditions throughout the tests. Complementary to these statistical analyses, the Fourier transforms of the surface elevation signals (Fig. 4 bottom) confirm the well-established spectral characteristics of the waves during the experiments at the wave frequency.

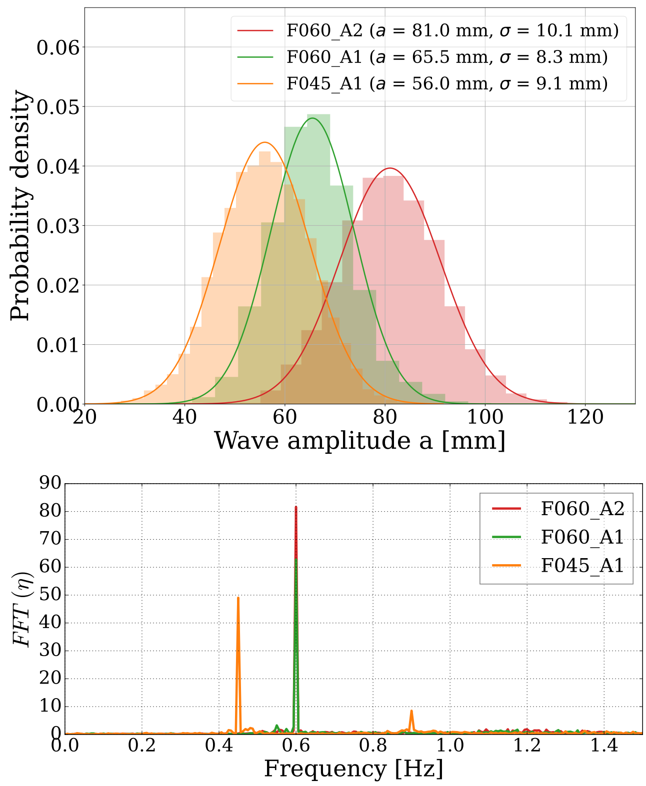

Fig. 4. Top: probability density functions of the wave amplitudes a = H/2, for the three cases with the turbine operating at TSR = 2.2. A Gaussian model is fit with the distribution. Bottom: Fourier Transforms of the surface elevation η for the three wave cases.

III. Turbine response under the waves propagation

A. Influence of the waves on the turbine performance

Fig. 5 presents the normalized power coefficient C_p curves (defined in Eq. 3) of the turbine for the three wave conditions, along with a reference steady case (REF) without waves. It is observed that the presence of waves barely affects the average $\overline{C_p}$ below the optimal TSR, while a significant distinction appears around and after the optimum operating point. Additionnally, the Fluctuation Intensity (FI, Eq. 3) of C_p is displayed, highlighting the impact of wave-induced unsteadiness on the power output. The results indicate a notable increase in power fluctuations in the presence of sur-

TABLE I
WAVE PARAMETERS AVERAGED OVER THE TEST DURATION. THE CORRESPONDING REAL SEA CONDITIONS ARE INDICATED IN BRACKETS.

Wave case	Period T [s]	Wave height H [m]	Wavelength λ [m]	h/λ	H/λ	KC
F045_A1	2.22 (10)	0.12 (2.2)	9.7	0.21	0.012	0.17
F060_A1	1.67 (8)	0.13 (2.6)	6.5	0.31	0.020	0.12
F060_A2	1.67 (8)	0.16 (3.2)	6.5	0.31	0.025	0.15

face waves, reaching up to 25% of the $\overline{C_p}$ at the optimal TSR for the F060_A2 case. Similar levels of fluctuations are observed between the cases F060_A1 and F045_A1 (15% to 20%), despite the F045_A1 case exhibits wave amplitudes approximately 15% lower than those in F060_A1.

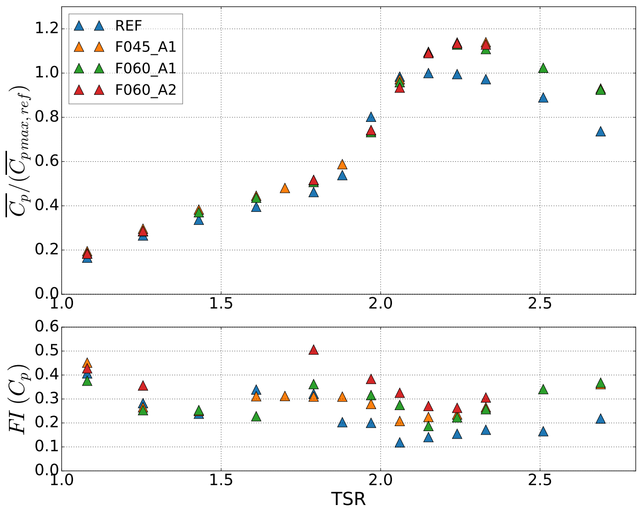

Fig. 5. $\overline{C_p}/\overline{C_p}_{max,ref}$ and the FI(C_p) curves for the reference case (no wave) and the three wave conditions. $\overline{C_p}_{max,ref}$ is defined as the maximum power coefficient obtained without waves.

$$C_p(t) = \frac{Q(t)\ \omega(t)}{\frac{1}{2}\ \rho\ S_{ref}\ U_0^3} \quad , \quad FI(C_p) = \frac{\sigma(C_p)}{\overline{C_p}} \qquad (3)$$

Based on these observations, a TSR of 2.05 is selected for the remainder of the study as a representative operating point for the study of C_p fluctuations. For this TSR, the fluctuations vary according to the wave conditions but for a similar $\overline{C_p}$. It makes it possible to avoid the potential impact of extracted power.

Fig. 6 presents the phase-averaged torque distribution for a rotor column, along with the Fourier transforms of the temporal signals in order to examine the impact of wave motion on the turbine output. The figures highlight the turbulent effects associated with the passage of the six blades, an already-documented phenomenon in previous studies [12]. Indeed, the harmonic peaks of the rotational frequency are observed (around 3 to 6 times f_ω), corresponding to the transitional phase of the spectral components from $6f_\omega$ to $3f_\omega$ around the chosen TSR, as related in [13]. Moreover, the wave influence is clearly demonstrated, with a high-intensity peak at the wave frequency. The peak balances with the turbulent components for the $F045\_A1$ and the $F060\_A1$ cases, and becomes the main torque component for the $F060\_A2$ case. The observations are in line with the power fluctuations previously found, indicating a strong influence of the wave cases and correlating the relative impact to one another.

In order to improve knowledge on the power fluctuations and its predictability for sustainable power exploitation, the next sections focus on representing the wave-related torque $Q_{wave}(t) = \overline{Q} + q_{wave}(t)$ evolution (with q_{wave} representing the torque fluctuation at the wave frequency) regarding the wave-induced velocity fluctuations U_{wave}.

B. Consideration of the wave frequency signature for the torque reconstruction

A deeper understanding of the power fluctuations is crucial for improving power predictability and grid integration. Therefore, the following sections focus on characterizing the evolution of the torque as a function of the wave-induced velocity fluctuations. With regard to the wave effects on the torque distribution, the results with the F060_A2 wave case are presented to illustrate the method. Similar results are obtained by studying the other wave cases.

Experimental and theoretical determination of the orbital velocity profile

PIV measurements are carried out upstream of the rotor column in order to temporally define the inlet flow velocity. Fig. 7 displays the velocity profiles at three positions in the plane. The differences emphasize the inductive effect of the turbine, with a decrease of 7% of the mean velocity profiles from x/D_e=-0.6 to x/D_e=-0.4. The orbital velocity profile u_{wave} is deduced from these planes by considering the velocity signals at the spectrum range around the wave frequency [f_{wave} - 0.05 ; f_{wave} + 0.05]. Fig. 8 presents the amplitude of the orbital velocity measured for the rotor column height, showing that the same profile is obtained regardless of the x-positions tested in the plane. While comparing the orbital velocity with the mean profiles, the orbital velocity represents about 20% to 30% of the global velocity values.

It is then deduced that the inductive effects do not alter the average wave effect on the water column. With regard to the profiles similarity in the PIV plane, the experimental velocity is taken at x/D_e=-0.4 in the following. In the same way, during the tests, the measurements of the free surface elevation carried out with the wave gauges make it possible to determine the theoretical Airy wave profile associated to the experimental case. By comparing the results, it appears that the average orbital velocity is correctly reproduced with the Airy theory.

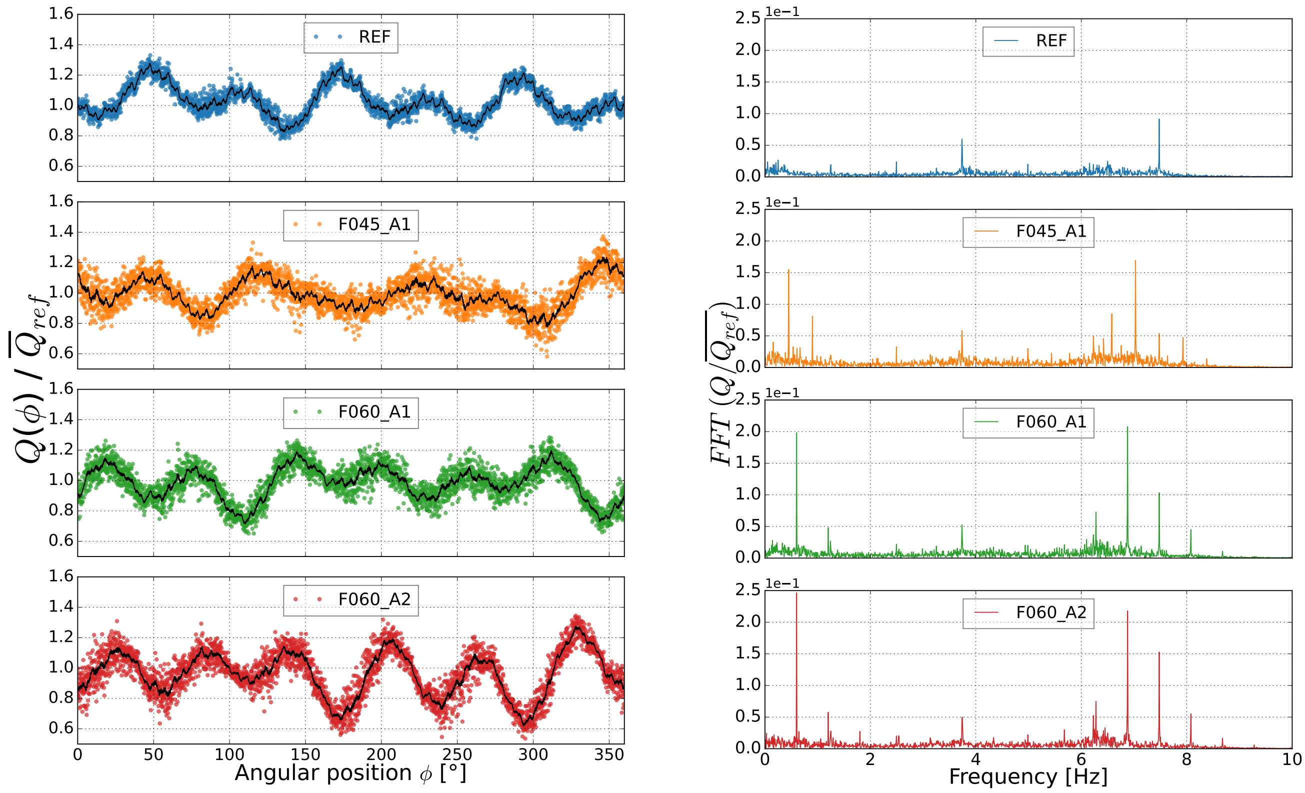

Fig. 6. Left side: turbine rotational phase-averaged Q angular distribution for the three wave cases and the reference case (TSR = 2.05, f_ω = 1.25 Hz). The mean component is represented by the black line.The colored dots are the measured $Q/\overline{Q}_{ref}$ values. Right side: Fourier transforms of the torque signals.

Due to the sampling frequency of the PIV setup, the studied signals (torque and velocity) are resampled to the same frequency base (torque signal interpolation at f_s = 15 Hz).

Response Amplitude Operator approach

To bring a first representation of the wave impact on the torque output, an analogous approach of the Response Amplitude Operator (RAO) is proposed, close to the one presented in [14]. The method is based on the assumption that torque and velocity at the wave frequency are highly coherent, which can be experimentally observed [9]. To do so, both signals are first filtered around the wave frequency using a band-pass filter centered at f_{wave}, similar to the process applied for the PIV measurements. This filtering isolates the wave-induced contributions while minimizing interference from other frequency components, especially the turbulent components. In comparison with the method presented in the above-mentioned study, which relies on power spectral density (PSD) ratios, the present approach uses the Fast Fourier Transform (FFT). The choice is made to retain both amplitude and phase information at the wave frequency, which is particularly relevant in the case of regular or narrow-band wave forcing. From this approach, a deterministic relationship between wave-induced velocity and torque can be established. In this framework, the velocity component induced by the waves U_{wave} is assumed to be proportionally related to the torque evolution Q_{wave} at the wave frequency. This relationship is quantified through average ratios of amplitude and phase, defined as: $r(f_{wave}) = \frac{|fft(Q_{wave})|}{|fft(U_{wave})|}$ and $\varphi(f_{wave}) = angle(\frac{fft(Q_{wave})}{fft(U_{wave})})$. The mean amplitudes and phases ratios provide coefficients defining the transfer function : $RAO(f_{wave}) = r(f_{wave}).e^{i\varphi(f_{wave})}$. These coefficients can be calculated by first rephasing the two signals on the basis of their cross-correlation. This function thus characterizes the sensitivity of the torque response to wave-induced velocity variations. The computed values are given in Table II, quantifying a global dependency of the torque response on wave conditions.

TABLE II
AMPLITUDE COEFFICIENTS DEFINED BY THE RATIO BETWEEN THE AVERAGE PARAMETERS FILTERED AROUND THE WAVE FREQUENCY.

Parameters	$r(f_{wave})$ [N.s]	$\varphi(f_{wave})$ [rad]
$Q_{wave}\ /\ U_{wave}$	14.3	0.07

Fig. 9 presents a temporal comparison between the reconstructed torque signal and the experimental measurements. From the velocity measurements, the reconstructed signal successfully captures the overall trend of the experimental torque while filtering out high-frequency turbulent peaks associated with blade passage effects. However, it tends to overestimate extreme values encountered, particularly at the peaks and troughs of the sines oscillations. Fig. 10 further illustrates this phenomenon by displaying the phase-averaged distribution of the wave-induced torque

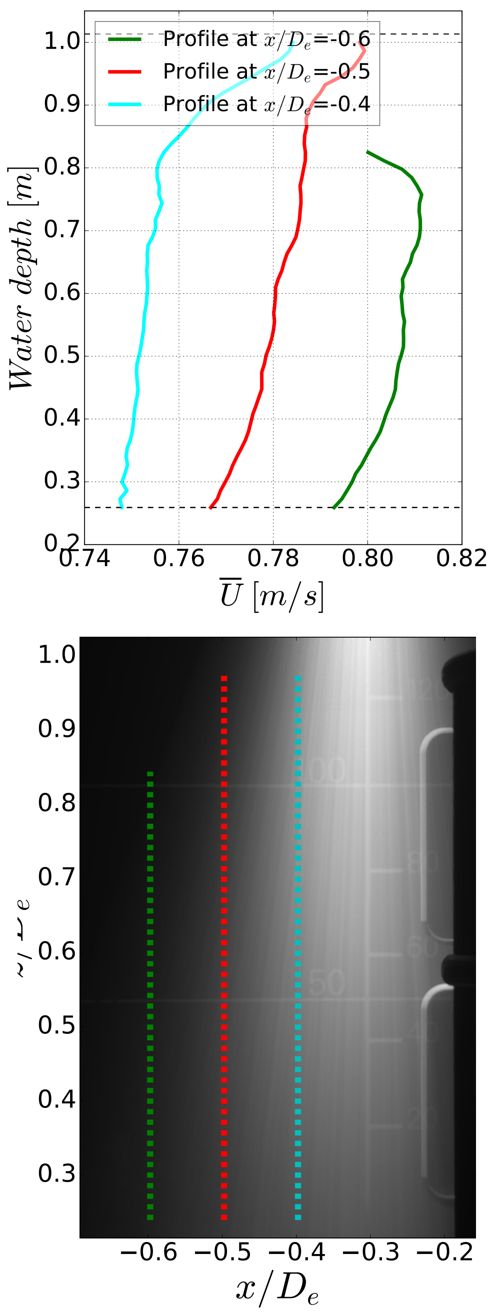

Fig. 7. Top: velocity profiles $\overline{U}$ extracted from PIV measurements. Bottom: PIV plane (y/D_e=0.37, half-width of the rotor column) with indications of the zones from which the velocity profiles are extracted. The green profile is cut off due to low light intensity in the top left corner of the image.

fluctuations, compared to the phase-averaged reconstructed torque. A noticeable hysteresis effect is observed on the measured data throughout the entire wave velocity cycle $U_{wave}(\phi)$ [15], which is not accounted for in the current RAO transfer function. The offset, which is up to 10-15% of the average torque, contributes to the discrepancies observed between the experimental and reconstructed signals in the time-domain representation. Overestimations of the extrema are noticeable, as the reconstructed torque signal is out of the elliptical bounds characterizing the filtered torque response.

To further characterize the turbine output fluctuations, we seek to better capture the hysteresis effects induced by the waves. Since a direct correlation between velocity and torque does not fully account for these phase-dependent variations, a more advanced formulation is required to accurately represent the torque response.

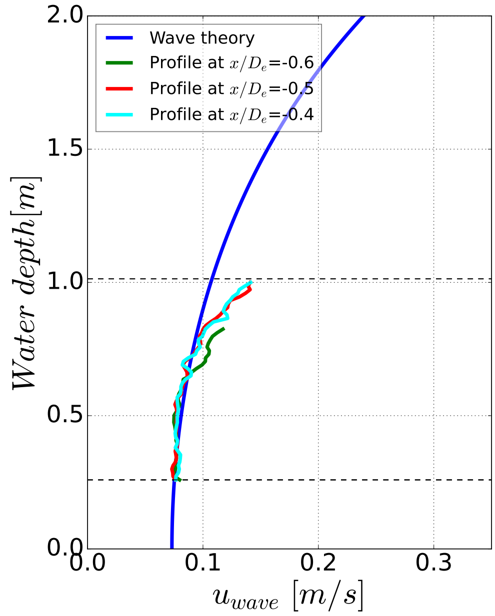

Fig. 8. Orbital velocities extracted from PIV measurements and from the Airy formulation (blue profile).

IV. Parametric formulation of the wave effect

Building on the previous analyses, which pointed out the predominant role of orbital wave velocity in torque fluctuations, the next step aims to develop a more accurate model of its influence on the turbine. A Morison-based formulation is applied to describe the torque response, comparing experimental velocity data with theoretical predictions from Airy wave theory.

A. Standard Morison formulation applied to the torque

To characterize the torque fluctuations of the rotor column, a Morison's loading formulation is adapted to the column torque. With this approach, the torque distribution is decomposed as a combination of a quadratic velocity term, commonly used for steady-state flow, and an inertial term which accounts for the acceleration of the wave-induced velocity. The latter is associated to an inertial coefficient named C_{MQ}, specific to the turbine configuration and operating conditions. The resulting formulation is expressed as Eq. 4:

$$Q(t) = \frac{1}{2}\ \rho\ S_{ref}\ R\ C_Q\ |U_{wave}(t)|^2 + \rho\ V_{ref}\ R\ C_{MQ}\ \frac{dU_{wave}(t)}{dt} \qquad (4)$$

The equation can be first solved by extracting the orbital velocity profile from PIV measurements taken upstream of the turbine. Second, a theoretical Airy

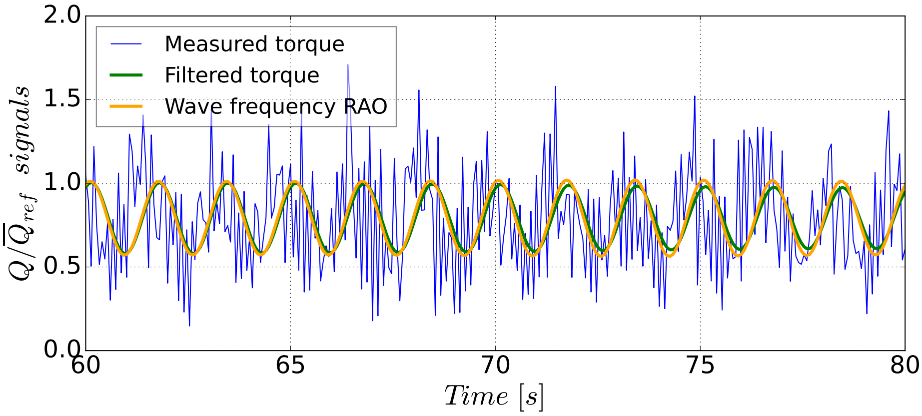

Fig. 9. Comparison of the experimental (blue and green) and reconstructed (orange) torque signals over a time range. The reconstructed torque is obtained using the transfer function establishment at the wave frequency.

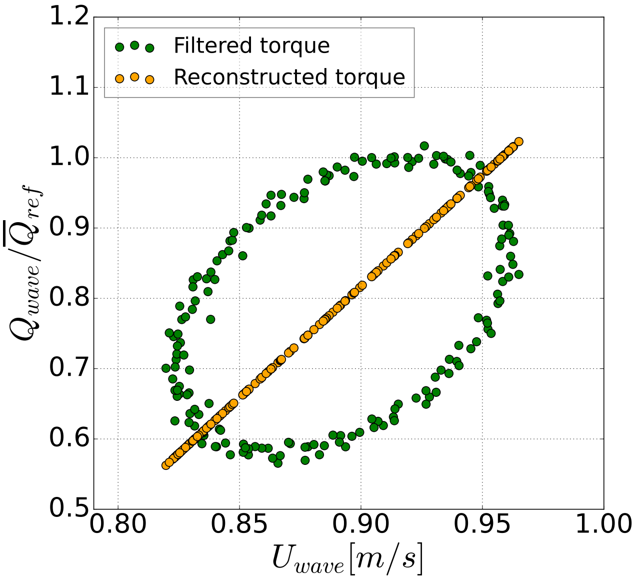

Fig. 10. Phase-averaged distribution of the experimental and reconstructed torque (Q_{wave}) at the wave frequency.

velocity is defined from the free surface elevation measurements (thus the wave characteristics) and applied to the proposed formulation. The approach adopted here consists of computing, for each time step, the depth-averaged wave velocity and acceleration over the turbine height. This enables the determination of the coefficients for this specific case (given the flow direction, velocity, and turbine operating point) using a non-linear least squares optimization method. The resulting coefficients deduced using the Airy theory are given in Table III. For the studied case $F060\_A2$, it can be noted that both coefficients are of the same order of magnitude.

Fig. 11 and 12 present the wave-filtered torque distribution, Q_{wave}, as a function of the wave-induced velocity, U_{wave}, for TSR = 2.05. Both parametric formulations, based on PIV and Airy orbital velocity profiles, exhibit a similar trend, effectively capturing the inertial effects on the torque distribution. The 10% inertia-related fluctuations are correctly reproduced at its higher, i.e. around U_{wave} = 0.89 m/s. For the future

TABLE III
COEFFICIENTS VALUES C_Q AND C_{MQ} OBTAINED FROM THE EQ. 4 SOLVING FOR THE DIFFERENT WAVE CASES. THE AIRY PROFILE IS CONSIDERED FOR THE VELOCITY-RELATED INPUT.

Wave case	C_Q	C_{MQ}
No wave	1.1×10^{-1}	-
F045_A1	1.0×10^{-1}	4.5×10^{-2}
F060_A1	1.0×10^{-1}	7.3×10^{-2}
F060_A2	1.0×10^{-1}	7.1×10^{-2}

studies, it is assumed as valid to define the orbital velocity profile using Airy's wave formulation.

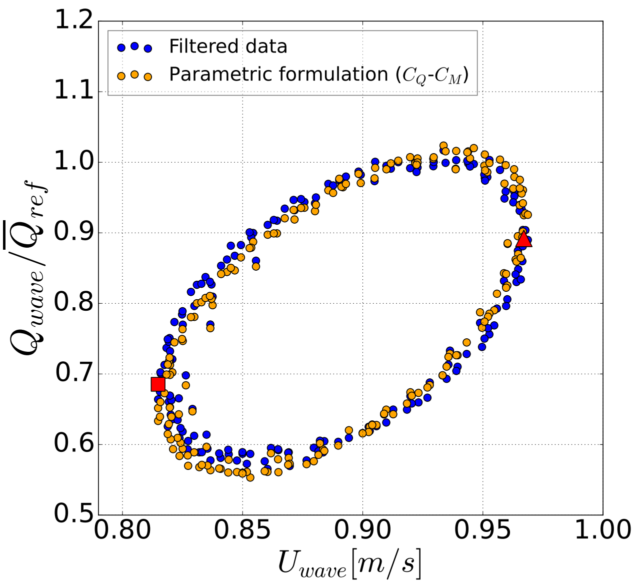

Fig. 11. Wave phase-averaged representation of the filtered torque fluctuations depending on the wave-induced velocity evolution and on the formulation applied with the experimental velocity measurements filtered at the wave frequency. The red square and triangle symbols represent two phase instants from the experimental data, which are phase-shifted by $\phi_{lag} = \pi$.

Although the parametric model provides a reasonable representation of the torque fluctuations induced by waves, some discrepancies remain, particularly in capturing the torque extrema. The quadratic velocity term alone does not fully account for these peaks, lead-

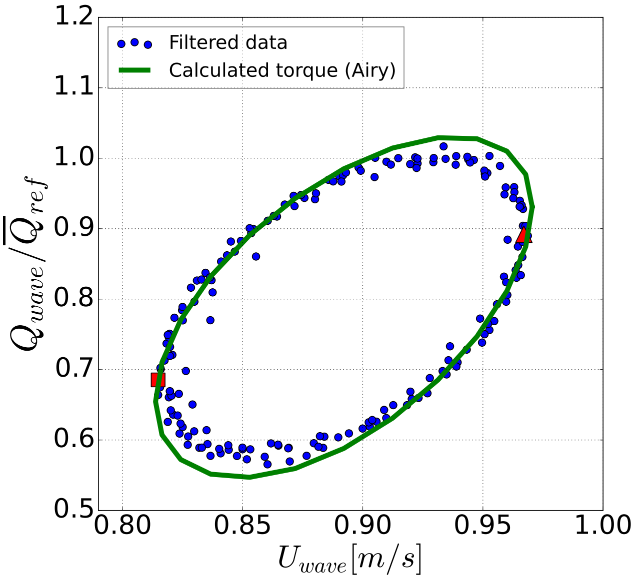

Fig. 12. Wave phase-averaged representation of the filtered torque fluctuations depending on the wave-induced velocity evolution and on the formulation applied with the theoretical Airy velocity. The red square and triangle symbols represent two phase instants from the experimental data, which are phase-shifted by $\phi_{lag} = \pi$.

ing to deviations of 8% at the minimum and 6% at the maximum. The general trend of the torque distribution aligns with the expected evolution, with torque maxima corresponding to velocity values slightly below the absolute velocity extrema.

To further investigate the relationship, Fig. 13 presents the phase averaged torque distribution as a function of the orbital acceleration $a_{wave} = \frac{dU_{wave}}{dt}$. According to Airy wave theory, the velocity and acceleration of an orbital particle are defined from related expressions $U_{wave} = U_0.cos(\omega t)$ and $a_{wave} = -U_0.\omega.sin(\omega t)$, implying a 90^o phase shift ($\frac{\pi}{2}$ rad) between the two terms.

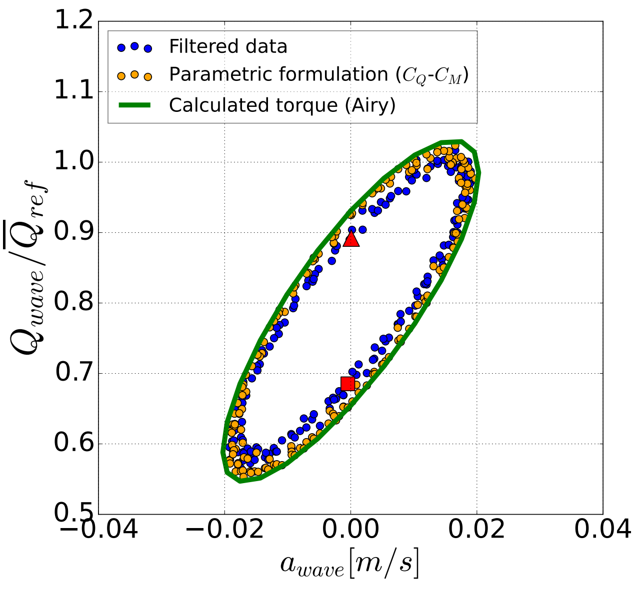

Fig. 13. Wave phase-averaged representation of the filtered torque fluctuations depending on the wave-induced acceleration.

This phase shift is well reproduced on elliptical distributions, where the torque evolution follows the expected pattern dictated by the inertia-related formulation. The comparison of phase instants in Fig. 11 and 13, through corresponding symbols separated by a phase lag of π rad, shows that the zero-crossings of the acceleration coincide with velocity extrema, and are slightly out-of-phase with the torque extrema (as defined previously from $\varphi(f_{wave})$).

The proposed model correctly represents the inertial effect on the torque fluctuations, while torque peaks are less well represented by the quadratic term, with under/over-estimates of around 5%.

While comparing the deduced coefficient with the case without wave, the same average C_Q value is found for the whole range of wave cases. The parametric model correctly represents the quadratic relation between mean velocity and torque evolution, which can explain that the average power coefficient is perceived as similar in Fig. 5. The coefficient C_{MQ} appears to be positive at this TSR, the inertial term thus variates in the same way than the acceleration term.

Representation regarding the operating points

To evaluate the influence of the TSR on the accuracy of the model, the approach is extended to two additional operating points: TSR = 1.8 and TSR = 2.2.

Fig. 14 and 15 compare the filtered torque fluctuations obtained from experimental measurements with those predicted by the Airy-based model. For TSR values lower than 2.0, the model accurately represents torque fluctuations, with deviations remaining below 5%. However, for TSR = 2.2, significant discrepancies arise. The elliptical orientation observed in the experimental data is not reproduced, and thus torque extrema are underestimated, with deviations reaching 15%.

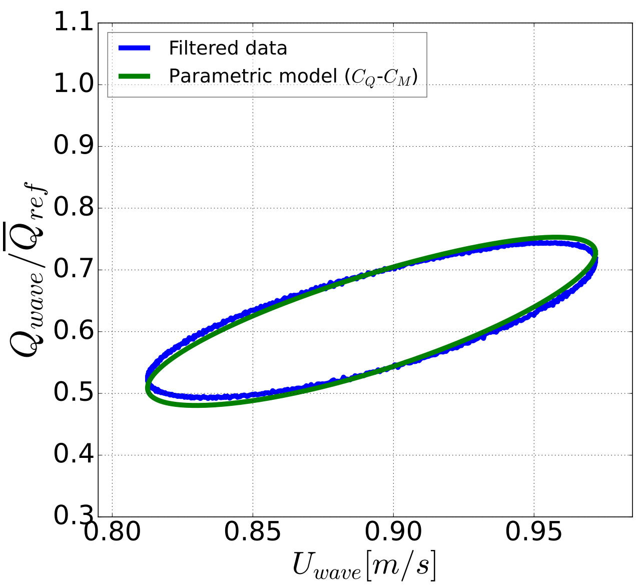

Fig. 14. Wave phase-averaged representation of the filtered torque fluctuations as a function of wave-induced velocity variations for TSR = 1.8. The models are established by considering the theoretical Airy velocity profile.

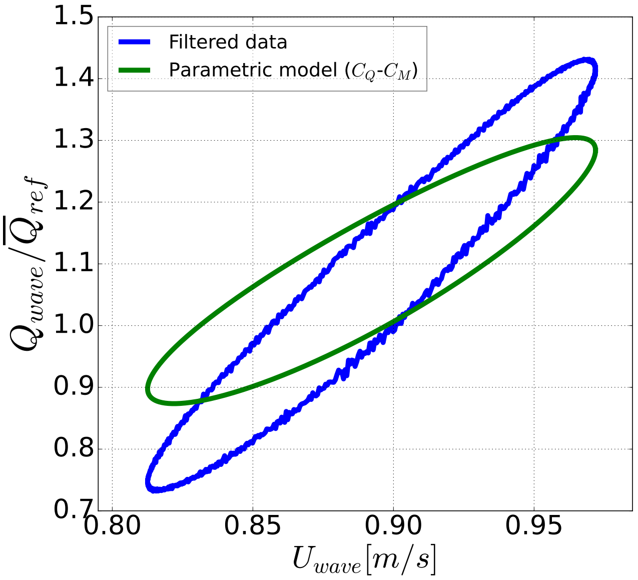

Fig. 15. Wave phase-averaged representation of the filtered torque fluctuations as a function of wave-induced velocity variations for TSR = 2.2. The models are established by considering the theoretical Airy velocity profile.

These differences highlight a limitation of the current modelling approach. The parametric model assumes a constant operating point, using a single C_Q coefficient for the entire range of encountered velocities. Actually, variations in TSR occur due to the unsteadiness imposed by the flow conditions and the turbine control. A more refined approach should incorporate these TSR variations by introducing an additional term related to the rotational speed. This enhancement would improve the model's ability to capture the overall trend of torque fluctuations with a better precision.

V. Conclusion

This study provides a detailed experimental investigation of the surface waves impact on the performance of a quadrirotor twin vertical axis tidal turbine. Controlled tests conducted in a wave-current flume tank demonstrate that waves affect the turbine's production with fluctuations up to 30% of the average power, which is deeply investigated around its optimal operating point in this study.

Spectral and phase-averaged analyses confirm a strong correlation between wave-induced velocity fluctuations and torque oscillations, emphasizing the need for a refined predictive approach to better define the output fluctuations. Specifically, it was shown that assuming the transfer function between velocity and torque at the wave frequency does not capture the inertial effects induced by wave motion. The standard Morison-based parametric model effectively accounts for the inertial contribution while distinguishing it from turbulence-related effects. However, discrepancies remain in the representation of torque extrema, with differences ranging from 10 to 15% between the filtered data and the model regarding the working TSR. This underscores the need for further refinements to fully account for nonlinear hydrodynamic interactions. The theoretical definition of the orbital velocity profile is in good agreement with the experimental data upstream of the turbine, as the Airy theory can be applied based on the free surface elevation measurements. Following studies on an extended modelling approach would lead to a high-fidelity evaluation by considering the variations in rotational speed and thus of the operating point.

These findings offer crucial insights for improving the turbine control strategies and improving energy yield predictions in real deployment scenarii. Future work will aim to study the output fluctuations for a wider range of operating conditions including flow velocity, direction, and wave characteristics. By doing so, a more accurate determination of the turbine behaviour in realistic offshore environments can be achieved, contributing to the development of more efficient and resilient tidal energy systems.

Acknowledgement

The authors acknowledge Jean-Valéry Facq and Cédric Derveaux for the model design, as well as Christophe Penisson and Benoit Gomez for their help during the tests and the data analysis.

References

[1] T. Jaquier, "Hydroliennes à flux transverse : développement d'un prototype HARVEST en canal," Theses, Université de Grenoble, Dec. 2011. [Online]. Available: https://theses.hal.science/tel-01424843

[2] Z. Zhang, Y. Zhang, Y. Zheng, J. Zhang, E. Fernandez-Rodriguez, W. Zang, and R. Ji, "Power fluctuation and wake characteristics of tidal stream turbine subjected to wave and current interaction," *Energy*, vol. 264, p. 126185, 2023. [Online]. Available: https://www.sciencedirect.com/science/article/pii/S0360544222030717

[3] R. Huang, S. Wang, Y. Lu, J. Tang, and W. Guo, "Research on bidirectional fluid-structure interaction characteristics of horizontal axis tidal turbines under wave current conditions," *Ocean Engineering*, vol. 294, p. 116806, 2024. [Online]. Available: https://www.sciencedirect.com/science/article/pii/S0029801824001434

[4] J. McNaughton, F. Zilic de Arcos, C. Vogel, and R. Willden, "Dynamic loading of two side-by-side tidal stream turbines in regular waves," *Journal of Fluids and Structures*, vol. 133, p. 104259, 2025. [Online]. Available: https://www.sciencedirect.com/science/article/pii/S0889974624001932

[5] M.-A. Dufour, B. Gaurier, G. Germain, and G. Pinon, "Experimental study of surface wave effects on a horizontal axis tidal turbine: loads and wake dynamics investigation," *Journal of Ocean Engineering and Marine Energy*, 2026.

[6] R. Linant, Y. Saouli, G. Germain, and G. Maurice, "Experimental study of the wave effects on a ducted twin vertical axis tidal turbine wake development," *Journal of Marine Science and Engineering*, vol. 13, no. 2, 2025. [Online]. Available: https://www.mdpi.com/2077-1312/13/2/375

[7] R. Martinez, S. Ordonez-Sanchez, M. Allmark, C. Lloyd, T. O'Doherty, G. Germain, B. Gaurier, and C. Johnstone, "Analysis of the effects of control strategies and wave climates on the loading and performance of a laboratory scale horizontal axis tidal turbine," *Ocean Engineering*, vol. 212, p. 107713, 2020. [Online]. Available: https://www.sciencedirect.com/science/article/pii/S0029801820307010

[8] M. Moreau, G. Germain, and G. Maurice, "Misaligned sheared flow effects on a ducted twin vertical axis tidal turbine," *Applied Ocean Research*, vol. 138, p. 103626 (11p.), 2023. [Online]. Available: https://doi.org/10.1016/j.apor.2023.103626

[9] ——, "Experimental investigation of surface waves effect on a ducted twin vertical axis tidal turbine," *Journal of Marine Science and Engineering*, vol. 11, no. 10, 2023. [Online]. Available: https://www.mdpi.com/2077-1312/11/10/1895

[10] M. Ikhennicheu, G. Germain, P. Druault, and B. Gaurier, "Experimental study of coherent flow structures past a wall-mounted square cylinder," FRANCE, pp. 137–146, 2019.

[11] L. Furgerot, A. Sentchev, P. Bailly du Bois, G. Lopez, M. Morillon, E. Poizot, Y. Méar, and A.-C. Bennis, "One year of measurements in alderney race: preliminary results from database analysis," *Philosophical Transactions of the Royal Society A: Mathematical, Physical and Engineering Sciences*, vol. 378, no. 2178, p. 20190625, 2020. [Online]. Available: https://royalsocietypublishing.org/doi/abs/10.1098/rsta.2019.0625

[12] M. Moreau, G. Germain, and G. Maurice, "Experimental performance and wake study of a ducted twin vertical axis turbine in ebb and flood tide currents at a 1/20th scale," *Renewable Energy*, vol. 214, pp. 318–333, 2023. [Online]. Available: https://www.sciencedirect.com/science/article/pii/S0960148123007589

[13] Y. Saouli, B. Gaurier, G. Germain, R. Linant, and G. Maurice, "Experimental investigation of the flow direction effects on a quadrirotor vertical axis tidal turbine," 09 2023.

[14] B. Gaurier, G. Germain, and J.-V. Facq, "Determination of the response amplitude operator of a tidal turbine as a spectral transfer function," *International Marine Energy Journal*, vol. 5, no. 2, pp. 151–160, 2022. [Online]. Available: https://doi.org/10.36688/imej.5.151-160

[15] X. Guo, J. Yang, Z. Gao, T. Moan, and H. Lu, "The surface wave effects on the performance and the loading of a tidal turbine," *Ocean Engineering*, vol. 156, pp. 120–134, 2018. [Online]. Available: https://www.sciencedirect.com/science/article/pii/S0029801818301823